NeuroImage 311 (2025) 121179

Contents lists available at ScienceDirect

NeuroImage

journal homepage: www.elsevier.com/locate/ynimg

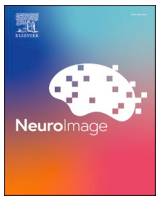

Enhancing cognitive abilities through transcutaneous auricular vagus nerve stimulation: Findings from prefrontal functional connectivity analysis and virtual brain simulation

Sora An [a], Se Jin Oh [b], Shinhee Noh [b], Sang Beom Jun [a,c,d,**], Jee Eun Sung [b,*]

[a] Department of Electronic and Electrical Engineering, Ewha Womans University, Seoul, Republic of Korea
[b] Department of Communication Disorders, Ewha Womans University, Seoul, Republic of Korea
[c] Graduate Program in Smart Factory, Ewha Womans University, Seoul, Republic of Korea
[d] Department of Brain and Cognitive Sciences, Ewha Womans University, Seoul, Republic of Korea

ARTICLE INFO

Keywords:
Transcutaneous auricular vagus nerve stimulation
Cognitive enhancement
Cognitive aging
Functional near-infrared spectroscopy
Virtual brain simulation

ABSTRACT

Recent studies have indicated the potential of transcutaneous auricular vagus nerve stimulation (taVNS) as an intervention for cognitive decline. In this study, we systematically analyzed the effects of taVNS on cognitive enhancement from the perspective of brain networks, by combining functional near-infrared spectroscopy (fNIRS) signal analysis with virtual brain simulations. Behavioral experiments with older adults demonstrated that participants with low baseline performance experienced significant improvements in working memory performance following taVNS, while those with high baseline performance tended to decline. This pattern was closely associated with functional connectivity (FC) in the prefrontal cortex (PFC) concurrently measured during the behavioral tasks, i.e., task performance correlated with FC in the PFC, particularly in the medial PFC (mPFC). Moreover, the changes in performance due to taVNS, which varied based on baseline performance, exhibited a notable alignment with the FC changes in the mPFC. These findings were further explored through virtual brain simulations. The simulation results demonstrated that the brain's functional state could vary depending on the network coupling parameter—capable of reflecting loss of structural brain connectivity associated with aging—and that the modulation effects induced by taVNS may also differ based on those functional states. Current results indicate that the efficacy of taVNS interventions for cognitive enhancement may vary according to the pre-intervention structural and functional states of individual brains. Therefore, the development of personalized optimization strategies for taVNS intervention is crucial, and digital brain research holds significant promise in advancing this field.

1. Introduction

Since clinical studies on vagus nerve stimulation (VNS) for treatment of refractory epilepsy or treatment-resistant depression have indicated the potential for improving cognitive function beyond regulation of major symptoms (Jodoin et al., 2018; Sun et al., 2017; Wang et al., 2024), VNS has been actively explored as an intervention of cognitive decline. Although its effectiveness for cognitive enhancement is somewhat controversial (Wang et al., 2024; Kong et al., 2024), studies in neurocognitive disorders such as Alzheimer's disease have reported significant benefits (Wang et al., 2024; Sjogren et al., 2002; Broncel et al., 2020).

Recent evidence suggests that non-invasive techniques like transcutaneous auricular vagus nerve stimulation (taVNS) can replicate the benefits of invasive VNS (Austelle et al., 2024; Badran and Austelle, 2022; Sharon et al., 2021). These findings have broadened the potential applications of VNS, leading researchers to investigate its effects on mild cognitive impairment (MCI) and cognitive function in healthy older adults (Jacobs et al., 2015; Wang et al., 2022; Trifilio et al., 2023; Naparstek and Yeh, 2023; Murphy et al., 2023). These studies overall

* Corresponding author at: Department of Communication Disorders, Ewha Womans University, 52 Ewhayeodae-gil, Seodaemoon-gu, Seoul 03760, Republic of Korea.
** Corresponding author at: Department of Electronic and Electrical Engineering and Adjunct Professor of Department of Brain and Cognitive Sciences, Ewha Womans University, 52 Ewhayeodae-gil, Seodaemoon-gu, Seoul 03760, Republic of Korea.
E-mail addresses: juns@ewha.ac.kr (S.B. Jun), jeesung@ewha.ac.kr (J.E. Sung).

https://doi.org/10.1016/j.neuroimage.2025.121179
Received 14 January 2025; Received in revised form 26 March 2025; Accepted 27 March 2025
Available online 28 March 2025

suggest a promising implication that non-invasive VNS may contribute to modulating cognitive decline, although heterogeneous outcomes were observed depending on the cognitive subdomains or the timing of assessments (i.e., acute or long-term effects).

Alongside the studies evaluating behavioral performance, neuroimaging research utilizing functional magnetic resonance imaging (fMRI), electroencephalography (EEG), or functional near-infrared spectroscopy (fNIRS) to explore the modulation effects of non-invasive VNS on brain networks has also been actively conducted (Badran et al., 2018; Fischer et al., 2018; Kamoga et al., 2024; Zhu et al., 2024). These studies have demonstrated significant changes induced by non-invasive VNS not only in brain regional activities but also in inter-regional functional connectivity (FC) through modulation of neuronal signaling via afferent pathways of the vagus nerve. However, considering the limitations in optimizing the efficacy of non-invasive VNS due to inter-individual differences, further research into the mechanisms of the VNS modulatory system is required.

Our previous behavioral study has revealed that the effects of taVNS in healthy older adults can vary depending on baseline performance; that is, the low-performance group demonstrated a significant improvement in cognitive ability following taVNS, while the high-performance group exhibited no significant changes or even a tendency to decline, depending on the type of cognitive task (Oh et al. submitted). This suggests that neurostimulation may lead to varied effects depending on the functional state of an individual's brain, which may explain the heterogeneous results observed in previous behavioral studies involving aging populations. Building upon our behavioral research, this study aims to systematically analyze the effects of taVNS on cognitive enhancement from the perspective of brain networks. In particular, we performed virtual brain simulations to investigate the effects of taVNS across various functional states of the brain, along with FC analysis using fNIRS. This novel approach demonstrates that the intervention effects of taVNS may depend on the pre-intervention brain state, thereby providing new insights into the mechanisms underlying cognitive modulation.

2. Materials and methods

2.1. Experimental design

The experimental data obtained from a total of 74 healthy older adults were used (Table 1) (Oh et al. submitted). Each participant performed behavioral tasks to evaluate working memory performance under both sham and active taVNS conditions during two visits, spaced at least one week apart. In the active session, taVNS was administered with a frequency of 25 Hz, a pulse width of 200 μs, and a 30-second on/off scheme (allears, TODOC, Seoul, Republic of Korea). taVNS was applied continuously, including for 15 min prior to the behavioral tasks (resting state) and while performing the tasks (a total of 40–45 min). The stimulation site was the cymba conchae of the left or right ear (Fig. 1A, Table 1), with counterbalancing applied, and the intensity was set between 2 and 4 mA taking into account each participant's pain threshold. In the sham session, taVNS was applied only during the first and last 30 s of the experimental session (Sun et al., 2021).

Table 1
Demographic characteristics of participants and changes in working memory performance following taVNS.

Group		Total (N = 74)	Low-performance group (N = 26)	High-performance group (N = 48)
Demographic data				
Age	Years, Mean (SD)	64.16 (3.99)	63.73 (4.31)	64.40 (3.83)
Gender	Male : Female	46 : 28	17 : 9	29 : 19
Education	Years, Mean (SD)	14.15 (3.00)	14.46 (2.96)	13.98 (3.04)
taVNS ear	Left : Right	37 : 37	15 : 11	22: 26
Task performance				
Accuracy (%) (Visuospatial 2-back)	Sham, Mean (SD)	75.61 (14.13)	59.79 (8.79)	84.19 (7.44)
	Active, Mean (SD)	77.03 (15.03)	69.76 (14.31)	80.97 (14.02)

Regarding the behavioral tasks, linguistic and visuospatial n-back tests (1-back and 2-back tasks) were employed, with the task order and the application sequence of sham/active sessions being counterbalanced across participants (Oh et al. submitted). The linguistic n-back task was modified from the SemBack version by Wright et al. (Wright et al., 2007), incorporating words from three semantic categories—animals, fruits, and clothing—with eight words per category, totaling 24 words. The visuospatial n-back task, adapted from Christensen and Wright (Christensen and Wright, 2010), comprised block stimuli consisting of four sets of three-dimensional colored cubes organized in different arrangements (Shepard and Metzler, 1971). Participants were required to respond (by pressing the spacebar) when the current stimulus was from the same category as the previous stimulus (1-back or 2-back) in the linguistic task, and when it precisely matched with the previous stimulus in the visuospatial task. Both tasks included 22 target stimuli from a total of 73 stimuli in the 1-back condition and 22 target stimuli from 84 stimuli in the 2-back condition. Stimuli were presented using E-prime software (version 2.0) (Walter et al., 2002; Schneider et al., 2002) with a stimulus onset asynchrony of 3500 ms, displaying each stimulus for 750 ms followed by a 2750 ms interstimulus interval (Wright et al., 2007) (Supplementary Figure 1).

To investigate the hemodynamics of the prefrontal cortex (PFC) during the experiment, fNIRS signals were recorded using the OEG-SpO2 (Spectratech Inc., Yokohama, Japan). The system consists of six sources and six detectors arranged at 3 cm intervals, forming a total of 16 measurement channels (Fig. 1A). The center of the bottom probe was located at the FpZ position in the international 10/20 EEG electrode system. The wavelengths of the near-infrared light used were 770 and 840 nm, and a sampling rate was 1.5259 Hz.

We categorized participants into low- and high-performance groups (Table 1) based on their behavioral task scores during sham stimulation, using the 95 % probability threshold of binomial distribution (high-performance group: correct responses $\geq$ 16 out of 22 target trials, low-performance group: 7 $\leq$ correct responses $\leq$ 15). This approach was motivated by our earlier observation that taVNS significantly enhanced performance only in the low-performance group. We used performance on the visuospatial n-back task as the basis for group division, as this yielded adequately sample sizes for statistical comparison (low-performance: n = 26; high-performance: n = 48 for visuospatial task; n = 13 and n = 56 for linguistic task). The experiment was conducted with the approval of the Ewha Womans University Institutional Review Board (No. 2022–0084), and all participants provided written consent prior to the experiment. For detailed experimental procedures, please refer to Oh et al. (submitted).

2.2. fNIRS data analysis

2.2.1. Pre-processing

The acquired fNIRS signals were preprocessed using the Homer3 MATLAB package (v1.80.2) (Huppert et al., 2009) according to the following steps (Lin et al., 2023) (Fig. 1B). First, channels identified as having poor quality were pruned from the raw light intensity signals (dRange=[0 10^{10}], SNRthresh=2, SDrange=[0.0 45.0]), and then the intensity signals were converted to optical density (OD). Motion artifacts

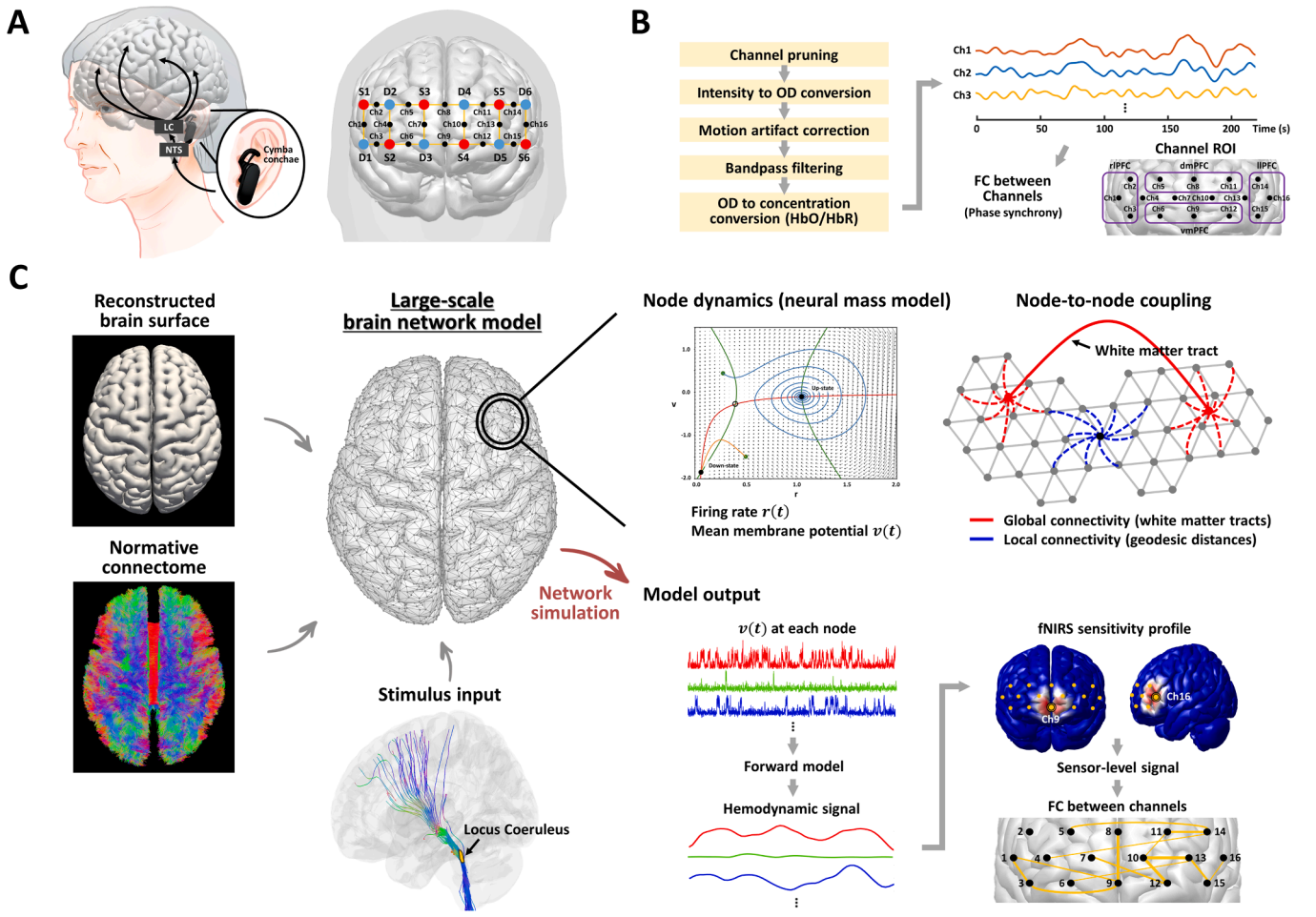

Fig. 1. Overview of the research methods. A. taVNS and fNIRS recording. Under both sham and active conditions for taVNS, fNIRS recordings were performed in the prefrontal region alongside the evaluation of working memory performance. The left figure shows the taVNS device used in the experiment and the target area of the cymba conchae, while the right figure illustrates the placement of optodes (red dots: sources, blue dots: detectors) and measurement channels (black dots) for fNIRS recordings. B. fNIRS signal analysis. Based on the preprocessed fNIRS hemodynamic signals following the procedure described in the left figure, FC analysis was performed. For the FC analysis between channel regions, four regions of interest (ROIs) were defined: vmPFC, dmPFC, llPFC, and rlPFC (purple squares). C. Virtual brain stimulation. The structural brain reconstructed from a standard brain MRI was re-sampled and constructed into a triangular mesh with 13,145 vertices. Each vertex (brain node) was equipped with a NMM that reproduces the activities of neuronal populations, and these brain nodes were coupled via two types of structural connectivity: 1) global connectivity based on a normative connectome (white-matter tracts; red lines), and 2) local connectivity based on the geodesic distance between nodes on the brain surface (blue lines). taVNS was applied by activating the white matter tracts projecting from the LC in the brainstem to other brain regions. The administered stimulation initially triggered changes in the directly stimulated region, and its effects propagated to other brain areas through inter-node interactions, inducing network effects at the whole-brain level. The activities in brain nodes obtained from network simulations under with and without taVNS conditions were converted into hemodynamic signals through a forward model, and then projected into the fNIRS channel space for comparison with empirical data. The simulated fNIRS signals were analyzed for FC using the same methods as in the empirical data.

in the converted OD were detected on a channel-by-channel basis (tMotion=1, tMask=1, STDEVthresh=50, AMPthresh=0.5) and corrected using wavelet transform (iqr=1.5). After the artifact removal, the OD signals were bandpass filtered between 0.01 and 0.1 Hz, and converted into concentrations of oxyhemoglobin and deoxyhemoglobin based on the modified Beer–Lambert law (Villringer and Chance, 1997).

2.2.2. FC analysis

Preprocessed hemodynamic signals from each measurement channel were used for FC analysis. For this analysis, oxyhemoglobin, known to be the most sensitive indicator of regional cerebral blood flow (Naito et al., 2024), was used, and the phase synchrony (PS) was employed as a measure of FC. The PS between two signals was defined as shown in Eq. (1) (Pedersen et al., 2018), where φ(t) represents the instantaneous phase extracted from each signal using the Hilbert transform, and T denotes the length of the signal. The PS takes values ranging from 0 to 1, with higher values indicating greater synchronization, and it was calculated for all pairs of channels.

$$PS_{i,j} = \frac{1}{T}\sum_{t=1}^{T}\left(1 - \left|\sin\left(\varphi_i(t) - \varphi_j(t)\right)\right|\right) \quad (1)$$

To compare the FC between the lateral PFC on both sides and between the dorsal and ventral regions in the medial PFC, four regions of interest (ROIs) were defined, each consisting of three measurement channels (left lateral PFC (llPFC); Ch 14, 15, 16, right lateral PFC (rlPFC); Ch 1, 2, 3, ventromedial PFC (vmPFC); Ch 6, 9, 12, dorsomedial PFC (dmPFC); Ch 5, 8, 11, Fig. 1B). The FC between the ROIs (llPFC↔rlPFC, vmPFC↔dmPFC) was defined based on the average values of FC from each channel pair.

The derived FCs were statistically compared via three-way mixed ANOVA with a group (low- and high-performance group), a taVNS condition (sham and active), and an ROI pair (llPFC↔rlPFC, vmPFC↔dmPFC) as independent variables. The group was designated as the between-subjects factor, while the taVNS condition and ROI pair were designated as within-subject factors. The significance threshold

was defined as $p < 0.05$, and post-hoc analyses were conducted using paired or independent samples *t*-tests with Bonferroni correction.

The FCs were further compared on a channel-pair-wise basis, using paired samples *t*-tests. In this case, corrections for multiple comparisons were not performed in order to examine the overall spatial characteristics of the channel pairs showing differences without disregarding potentially meaningful channel pairs. All statistical analyses described above were performed using IBM SPSS STATISTICS version 30.

2.3. Virtual brain simulation

2.3.1. Model construction

The virtual brain model was constructed based on a high-resolution modeling approach (An et al., 2022), utilizing the MNI ICBM 152 brain template (Fonov et al., 2009; Fonov et al., 2011) and normative connectome (Elias et al., 2024) (Fig. 1C). To achieve this, the first step involved reconstructing the cortical and subcortical surfaces from the T1-weighted MRI (MNI template) using Freesurfer (version v6.0.0) (FreeSurfer, 2012). The reconstructed brain surface was resampled into a triangular mesh consisting of 13,145 vertices and 25,877 faces, with an average distance of 5.60 mm between adjacent vertices.

Each vertex (brain node) was equipped with a neural mass model (NMM) replicating the macroscopic dynamics of neuronal populations (Fig. 1C). The Montbrió et al. model, a mean-field representation of an ensemble of infinitely connected quadratic-integrate-and-fire neurons, was used as the NMM (Montbrió et al., 2015; Lavanga et al., 2023; Fousek et al., 2022). The model is described by Eq. (2), and definitions of the model variables and parameters are provided in Table 2 (Montbrió et al., 2015; Hashemi et al., 2024; Rabuffo et al., 2021).

$$\begin{aligned}\tau \dot{r}_i(t) &= 2r_i(t)v_i(t) + \frac{\Delta}{\pi\tau} \\ \tau \dot{v}_i(t) &= {v_i}^2(t) - (\pi\tau r_i(t))^2 + J\tau r_i(t) + \eta + \xi_i(t) + I_{coup,i}(t) + I_{stim,i}(t)\end{aligned} \tag{2}$$

$$I_{coup,i}(t) = C\{\ \alpha\ I_{glob,i}(t) + (1-\alpha) I_{loc,i}(t)\ \} \tag{3}$$

$$I_{glob,i}(t) = \sum_{j=1}^{N} W_{glob,ij} r_j\left(t - d_{ij}\right) \tag{4}$$

$$I_{loc,i}(t) = \sum_{j=1}^{N} W_{loc,ij} r_j(t),\ \ W_{loc,ij} = \exp\left(-\frac{{g_{ij}}^2}{2\sigma^2}\right) \tag{5}$$

Table 2
Definition of variables and parameters in Montbrio's neural mass model.

Variables	Biophysical meaning	
r	Population firing rate	
v	Average membrane potential	
ξ	Dynamic random noise	
I_{coup}	Coupling input from other nodes	
I_{stim}	External stimulus input	
Parameters	**Biophysical meaning**	**Value**
J	Average synaptic weight	14.5
η	Average excitability	-4.6
Δ	Heterogeneous noise spread	0.7
τ	Characteristic time constant	1.0

The NMM at each node was coupled with other NMMs via structural brain connectome (I_{coup}, Eq. (3)), considering both global and local connectivity (Fig. 1C). Global connectivity was defined based on a normative connectome, consisting of 12 million white matter tracts assembled from 985 healthy adults' diffusion-weighted images (Elias et al., 2024). The coupling input due to global connectivity I_{glob} was defined as in Eq. (4), where W_{glob} represents the connection weight depending the number of fiber tracts between brain nodes, and d denotes the transmission delay proportional to the length of the fiber tracts. The transmission speed was set as 3 m/s, which is within a biologically plausible range (Trebaul et al., 2018). Local connectivity was defined based on the geodesic distance between nodes on the brain surface, reflecting the strong interaction among spatially close neuronal populations. The coupling input due to local connectivity I_{loc} was described in Eq. (5), where W_{loc} represents the connection strength with a Gaussian kernel applied to the geodesic distance g_{ij} ($\sigma = 8.0$ mm) (Spiegler et al., 2016). The ratio of global to local coupling was designated as 0.8:0.2 (i.e., $\alpha = 0.8$), and the network coupling parameter C, which controls the overall intensity of the coupling input for the NMMs, was systematically swept across a range of values.

2.3.2. Network simulation for taVNS

To simulate the network effects induced by taVNS, stimulation was applied by activating white matter tracts projecting from the locus coeruleus (LC), which is known as a major branch of the afferent pathway of the vagus nerve (Sharon et al., 2021; Hilz, 2022; Colzato and Beste, 2020) (Fig. 1C). The anatomical mask for the LC was used as provided by Levinson et al. 2023 (Levinson et al., 2023). Because a sufficient number of fiber tracts directly connecting the LC on both sides were identified, all fiber tracts projecting from both LC to other brain regions were activated, regardless of whether taVNS was applied to the left or right ear. In other words, stimulation was applied by providing immediate input in the form of a short pulse (200 μs) to the NMMs connected to the activated fiber tracts, and this stimulus input I_{stim} was repeatedly administered at a frequency of 25 Hz, consistent with the experimental environment.

Resting state activity was simulated for 10 min with taVNS and without taVNS conditions, respectively. Random noise inputs and the initial values of model variables were maintained consistently across both conditions to clearly ascertain the changes caused by taVNS.

2.3.3. Conversion to fNIRS hemodynamic signals

The electrical signals at each NMM acquired through network simulation were converted into hemodynamic signals using the Balloon-Windkessel model (Friston et al., 2003). The converted hemodynamic signals at each NMM were projected into the fNIRS measurement channel space identical to the experimental environment, i.e., 16 channels located in PFC. In this step, the sensitivity profile for each measurement channel was calculated based on Monte Carlo photon migration forward modeling using AtlasViewer software (Aasted et al., 2015; Pfeifer et al., 2018). The inset images in Fig. 1C show the sensitivity profiles for two example channels.

The simulated fNIRS signals were bandpass filtered from 0.01 Hz to 0.1 Hz, and FC analysis was conducted in the same manner as with the empirical data.

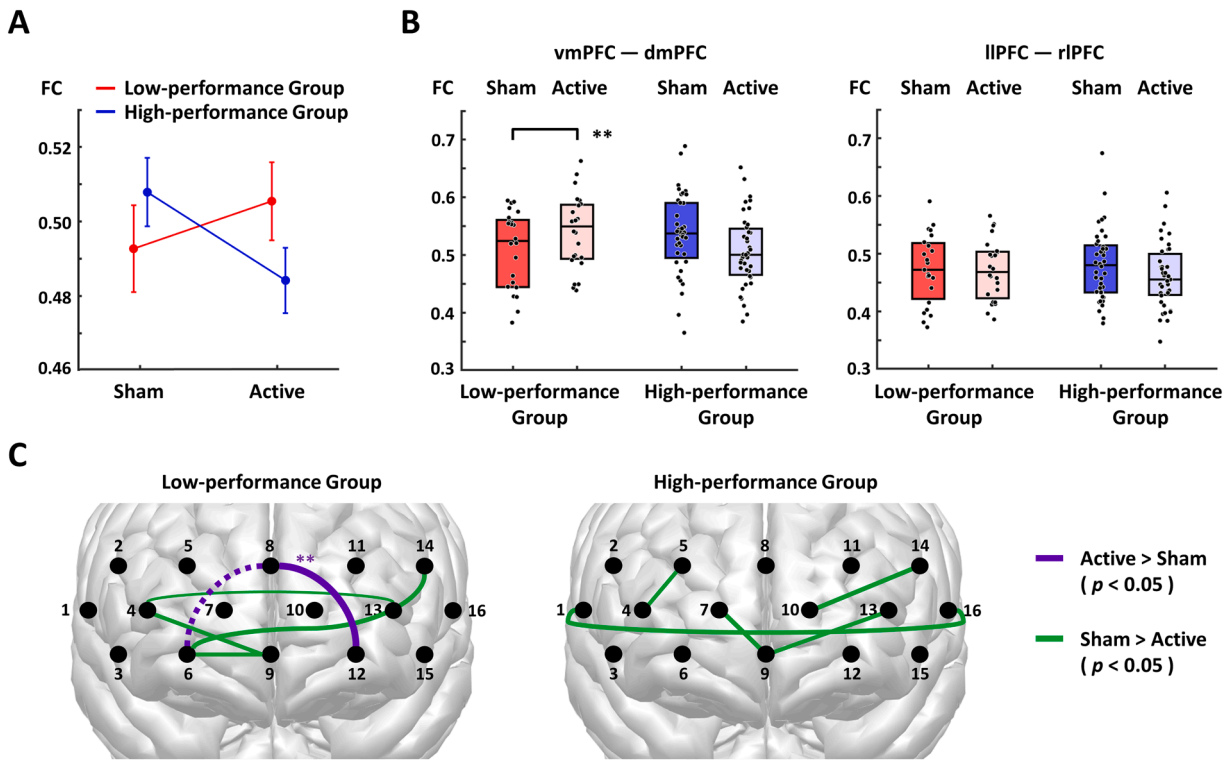

Fig. 2. FC analysis results of recorded fNIRS signals. A. Interaction between group and taVNS condition. Red and blue represent FC values (mean and standard error) in the PFC for the low- and high-performance group, respectively. B. Channel ROI pair-based FC analysis results. The figure shows FC values according to taVNS conditions (sham, active) in low- and high-performance groups. The left and right figures represent the results for the vmPFC↔dmPFC and llPFC↔rlPFC pairs, respectively, and double asterisks indicate significant differences at the $p < 0.01$ level. C. Channel-pair-wise FC analysis results. The figures display the (measurement) channel pairs that showed significant differences between taVNS conditions (sham, active) within each performance group. The purple lines indicate pairs that exhibited stronger FC in the active condition compared to the sham condition, while the green lines represent pairs that showed weaker FC in the active condition. Double asterisks denote significant differences at the $p < 0.01$ level, and the dotted lines represent the channel pair that was marginally rejected for significance ($p = 0.06$).

3. Results

3.1. FC analysis of fNIRS signals

Three-way mixed ANOVA (group * taVNS condition * ROI pair) revealed significant effects for: 1) the main effect of ROI pair ($F_{(1,61)} = 58.932$, $p < 0.001$, $\varepsilon^2 = 0.491$), 2) the interaction between group and taVNS condition ($F_{(1,61)} = 4.358$, $p = 0.041$, $\varepsilon^2 = 0.067$), and 3) the three-way interaction ($F_{(1,61)} = 6.045$, $p = 0.017$, $\varepsilon^2 = 0.090$). The main effect for the ROI pair was driven by greater FC between the vmPFC and dmPFC compared to the FC between the llPFC and rlPFC (vmPFC↔dmPFC = 0.524 ± 0.068, llPFC↔rlPFC = 0.473 ± 0.059). The significant two-way interaction was driven by differential group patterns per each condition, with the high-performance group showing higher FC in the sham condition but lower FC in the active condition (Fig. 2A).

As post-hoc analyses for the three-way interaction, two separate two-way ANOVAs were performed per each ROI pair. The interaction between group and taVNS condition was significant only in the vmPFC↔dmPFC ROI pair ($F_{(1,62)} = 9.368$, $p = 0.003$, $\varepsilon^2 = 0.131$). In the low-performance group, FC significantly increased in the taVNS active condition compared to the sham condition (sham = 0.509 ± 0.068, active = 0.540 ± 0.064, $p = 0.004$). In contrast, in the high-performance group, FC tended to decrease relative to the sham condition, although this change was not statistically significant (sham = 0.535 ± 0.069, active = 0.511 ± 0.068, $p = 0.062$) (Fig. 2B). No significant effects were found in the llPFC↔rlPFC ROI pair.

The channel-pair-wise FC analysis results are presented in Fig. 2C. The channel pairs exhibiting significantly higher FC in the active condition compared to the sham condition were identified only in the low-performance group, and these channel pairs were located between the dorsal and ventral regions in the mPFC. In the high-performance group, significantly lower FC was observed in several channel pairs, but no specific spatial pattern was identified. The channel-pair-wise results for group differences within the taVNS condition are provided in Supplementary Figure 2. In the sham condition, the high-performance group demonstrated higher FC compared to the low-performance group, especially in channel pairs in the mPFC. In the active condition, no particular pattern was observed in FC differences between groups; however, the high-performance group exhibited lower FC in a channel pair between the dorsal and ventral regions of the mPFC, as well as in a channel pair within ventral regions.

3.2. Virtual brain simulation for taVNS

The virtual brain model generated spontaneous network activities on a whole-brain scale, based on the intrinsic properties of each brain node and the inter-node coupling via the structural connectome. When taVNS was applied, brain nodes directly connected to the white matter tracts projected from the LC were immediately affected by the stimulation, and the impact propagated through inter-node interactions, thereby inducing modulation effects at the network level.

The network effects induced by taVNS were systematically investigated through a parameter sweep of the network coupling parameter C. Fig. 3A visualizes the mean difference in hemodynamic signals at each brain node with and without taVNS applied, across specific C values. When the C was low, indicating that the overall coupling strength of the network was weak, the effect of taVNS was restricted to the thalamus, amygdala, and some posterior areas of the superior frontal cortex where

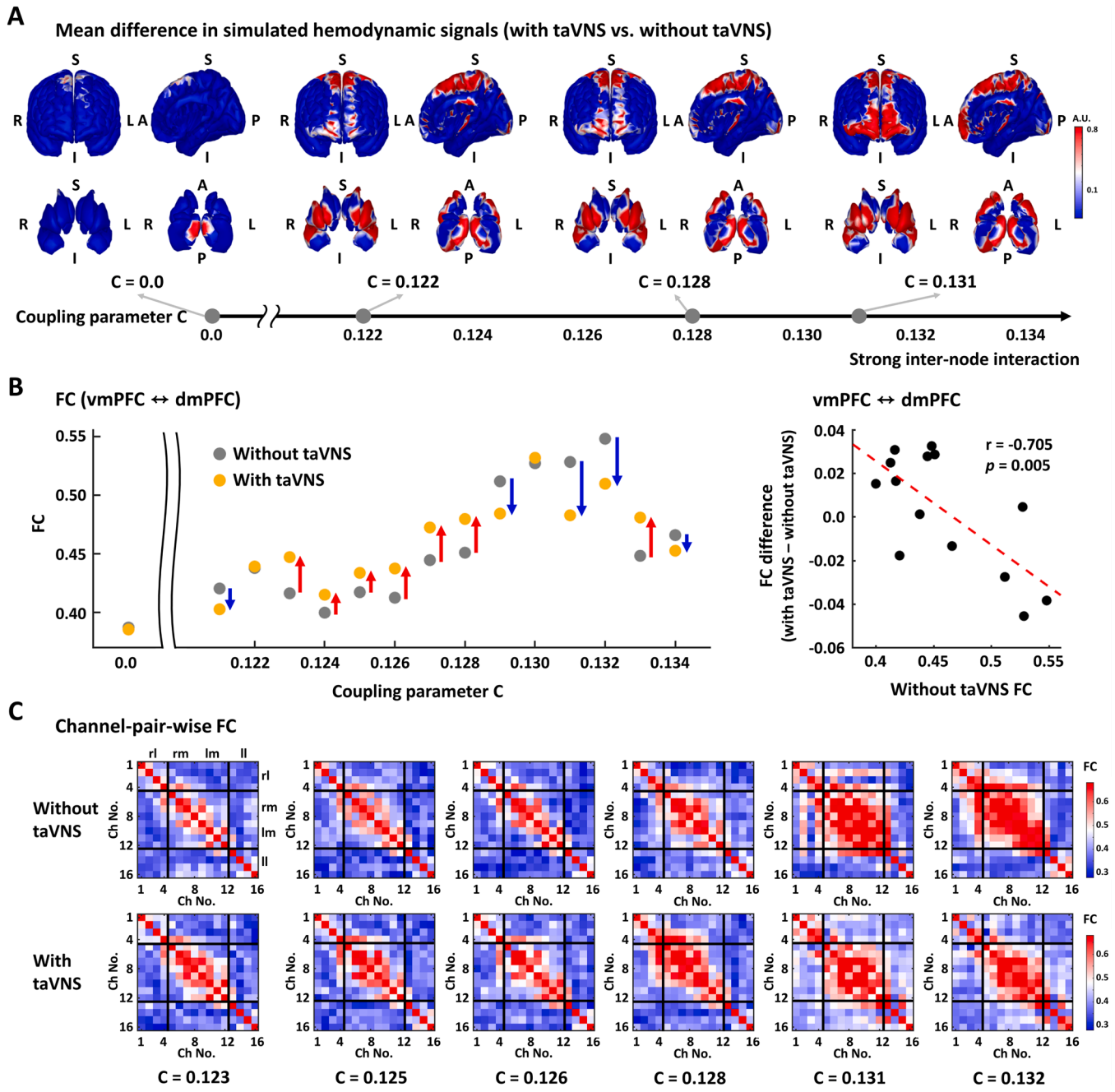

Fig. 3. Virtual brain simulation results. A. Changes in regional hemodynamic activities induced by taVNS. The figure illustrates the distribution of brain regions where activity changes are induced by taVNS, depending on the value of the network coupling parameter *C*, which regulates the overall strength of inter-node interactions in the model. The color code represents the average difference (absolute value) in simulated hemodynamic signals between the conditions with and without taVNS. Specifically, the red areas indicate regions that showed greater changes due to taVNS. B. Channel ROI pair-based FC analysis results of simulated fNIRS signals. The figure exhibits FC values between the vmPFC and dmPFC under conditions without (gray dots) and with taVNS (yellow dots), depending on the coupling parameter *C*. The red (blue) arrows denote enhanced (reduced) FC following taVNS. The right figure presents a scatter plot indicating the negative correlation ($p = 0.005$) between FC values under the without taVNS condition and the FC changes induced by taVNS. C. Channel-pair-wise FC analysis results of simulated fNIRS signals. The figure presents the channel-pair-wise FC (16 by 16 matrix) under conditions with and without taVNS across several values of *C*. rl: right lateral, rm: right medial, lm: left medial, ll: left lateral region.

the stimulus was directly applied. However, as the *C* increased, changes due to taVNS were observed across most subcortical areas (including hippocampus, amygdala and thalamus), the posterior cingulate cortex, the superior frontal cortex, and the PFC, particularly in the medial and ventral regions (Fig. 3A).

The results of the FC analysis in the fNIRS measurement channel space are presented in Fig. 3B First, after a certain level of coupling was applied to the model ($C \geq 0.123$), the FC between vmPFC and dmPFC tended to increase overall as the *C* increased. When taVNS was applied, in cases where the *C* was low (ranging from 0.123 to 0.128), the FC (vmPFC↔dmPFC) increased compared to the FC without taVNS (baseline FC); however, in cases where the *C* was high, i.e., when the baseline FC was already strong (ranging from 0.129 to 0.132), the FC showed no change or a rather decreasing pattern following taVNS. The right subplot in the Fig. 3B demonstrates a negative correlation between baseline FC and changes in FC (vmPFC↔dmPFC) induced by taVNS. Regarding the

FC between llPFC and rlPFC, a similar pattern was observed overall, although it was not as pronounced as that between vmPFC and dmPFC (Supplementary Figure 3).

The channel-pair-wise FC analysis results of simulated fNIRS signals are presented in Fig. 3C. The results indicate that 1) FC within the PFC (particularly between channels on the medial side rather than on the lateral side) is enhanced overall as the *C* increases, and 2) FC is strengthened by taVNS when baseline FC is weak, but weakened when baseline FC is strong.

4. Discussion

The current study systematically analyzed the effects of taVNS on cognitive enhancement from the perspective of brain networks. The fNIRS signal analysis indicated that FC in the PFC was associated with task performance in older adults. Particularly, FC within mPFC (vmPFC↔dmPFC) showed a stronger correlation, with the high-performance group (at the baseline) exhibiting relatively higher FC compared to the low-performance group. mPFC is a core hub of the default mode network (DMN) and has traditionally been understood as being activated at rest and inhibited during cognitive tasks. However, recent neuroimaging studies have provided accumulating evidence that mPFC also plays a crucial role in various cognitive functions, including working memory, long-term memory, attention, and decision-making (Hampson et al., 2006; Jobson et al., 2021; de Oliveira Jereissati et al., 2023). Moreover, FC alteration between mPFC and other cortical/subcortical areas have been consistently found across the progression of aging, neurocognitive disorders including MCI and Alzheimer's disease, as well as psychiatric diseases that are accompanied by cognitive deficits (Jobson et al., 2021; de Oliveira Jereissati et al., 2023; Andrews-Hanna et al., 2007; Xu et al., 2019; Dugré et al., 2021). This suggests that FC changes of the mPFC may serve as an important indicator for cognitive decline. Due to the limitations of our measurement environment restricted to the PFC, we were unable to analyze mPFC FC at the whole-brain network level. However, considering that the dmPFC has major connections to cortical areas while the vmPFC is primarily linked to the limbic system, and that both regions are highly interconnected with subcortical areas including the thalamus, hippocampus, and amygdala (Jobson et al., 2021), the decrease in FC between the dmPFC and vmPFC may imply a decline in the overall function of the frontal-subcortical circuitry.

Such a low FC between the dmPFC and vmPFC significantly increased due to taVNS, along with the improvement in task performance. This benefit from taVNS was observed only in the low-performance group. In the high-performance group, which had higher baseline FC (vmPFC↔dmPFC), both FC and behavioral performance showed a relative decrease during the taVNS active session compared to the sham session. These results indicate that when baseline FC is low, taVNS can lead to sequential involvement and entrainment along the afferent pathway of the vagus nerve (Broncel et al., 2020; Hilz, 2022; Colzato and Beste, 2020), enhancing synchronization in the PFC (especially in the medial part), whereas when baseline synchronization is high, the same conditions of taVNS may elicit neural desynchronization effects, as demonstrated in clinical studies on epilepsy that showed VNS can suppress on-going seizures (Boon et al., 2015) or induce EEG desynchronization (Vespa et al., 2021). This suggests that the modulation effects of taVNS may differ depending on the functional state of each individual's brain network.

Regarding the relationship between baseline behavioral performance and responses to taVNS, a recent study has reported findings that are contrary to the current results (Thakkar et al., 2025). They investigated the effects of taVNS on word learning and found a significant correlation between its efficacy and baseline verbal working memory performance, i.e., participants with higher baseline working memory performance demonstrated better outcomes in word learning with taVNS and retention one week later. However, it is important to note that the study focused on young adults, in contrast to the current study, which targeted older adults. The authors interpreted that the interaction between the existing working memory circuitry and the hippocampus engaged by taVNS may facilitate enhanced neural plasticity, leading to more rapid learning. However, in older adults, enhancing plasticity through neurostimulation may be more challenging compared to younger adults (Ghasemian-Shirvan et al., 2020). The age-related differences in the effects of taVNS should be systematically investigated in conjunction with neuroimaging studies. Furthermore, a comprehensive examination from multiple perspectives is required, encompassing both the targeted functional network and the translation into related networks.

Although fNIRS signal analysis yielded interesting results regarding the response to taVNS, it was restricted to only the PFC, which is closely related to cognitive functions. Therefore, we further performed high-resolution virtual brain simulations to explore the network effects at the whole-brain level induced by taVNS. The virtual brain model, constructed from the structural brain characteristics (anatomy and connectome) and equipped with NMM, enables the reproduction of the brain's functional properties, thereby enhancing our understanding of the underlying causes of functional changes based on interactions with structural characteristics (Lavanga et al., 2023; Martí-Juan et al., 2023).

In this study, we systematically examined taVNS-induced network effects according to the network coupling parameter *C*, which can reflect structural alterations related to aging. Numerous brain imaging studies have reported a loss of overall structural connectivity in the brain due to white matter degradation as aging progresses, and studies are also being conducted to clarify the relationship between this loss and functional alterations (Petkoski et al., 2023; Groh and Simons, 2024; Gunning-Dixon et al., 2009; Coelho et al., 2021). Given that each brain node in the model is coupled through structural connectivity, with the coupling strength scaled by parameter *C*, the *C* can be considered to reflect the loss of structural connectivity at the whole-brain level. That is, a smaller value of parameter *C* may indicate a more severe loss of structural connectivity due to aging.

The network simulations demonstrated that as the *C* decreases, coupling between brain nodes weakens, leading to reduced FC, which indicates that a weakening of structural connectivity may be associated with a decline in FC. This pattern was particularly pronounced in the FC between the vmPFC and dmPFC, although it was also observed between the left and right lPFC. This result is in line with previous brain imaging studies showing that the DMN involving the mPFC is most severely disrupted with the aging (Jobson et al., 2021; Andrews-Hanna et al., 2007).

The simulations applying taVNS demonstrated the modulatory pathway from LC in the brainstem to subcortical areas and PFC. In particular, when the coupling parameter *C* was small, the stimulation effects were limited to regions directly connected to the activated white matter tracts, whereas as the *C* increased, the effects propagated to other regions through strong inter-node interaction, ultimately reaching the PFC. The brain areas that exhibited changes following stimulation were similar to those where activity changes due to taVNS were observed in previous fMRI-based studies (Badran et al., 2018).

In terms of FC in the PFC, the effects of taVNS varied depending on the coupling parameter *C*. When the *C* was small (indicating a loss of structural connectivity) and the baseline FC was low accordingly, stimulation enhanced FC; however, when the *C* was high and the baseline FC was already elevated, the stimulation under the same conditions resulted in a decrease in FC. This pattern aligns well with findings from fNIRS measurements and reaffirms that the intervention effect of taVNS may differ depending on the functional state of the brain. Moreover, considering that such functional state could be affected by structural characteristics, we can speculate that individuals with lower baseline behavioral performance may have experienced relatively greater structural loss in white matter, contributing to a further decrease in baseline FC. A positive aspect of our current findings is that taVNS was

effective in those individuals. In other words, the results suggest that taVNS may provide greater benefits for individuals whose brain structural and functional decline has already progressed due to aging or cognitive impairment. Nevertheless, the aspects related to structural loss need to be further verified. Structural connectome analysis based on individual diffusion-weighted MRI will enable this.

The simulation results convey another important message. Given the degree of FC increase in the PFC due to taVNS, in cases of excessive loss of structural connectivity leading to significantly reduced baseline FC, achieving recovery to an adequate level may be challenging, even if FC improves following taVNS (please compare the improved FC values by taVNS in the *C* ranges of 0.123–0.126 and 0.127–0.128 in Fig. 3B). Therefore, the results suggest that early intervention could be effective in normalizing the functional state of the brain, considering that structural and functional alterations progress with aging.

The current study explored the intervention effects of taVNS concerning changes in brain network characteristics and their association with behavioral changes; however, it still has several limitations. Regarding the administration of taVNS in the experiment, participants were counterbalanced to receive stimulation on either the left or right ear. Studies to date have predominantly employed left ear stimulation due to safety concerns related to cardiac activity, but this practice has emerged from traditional cervical VNS. Considering the anatomical pathway of the auricular branch of the vagus nerve (ABVN), it has been indicated that taVNS may avoid the risk of adverse cardiac events; accordingly, recent studies have reported on the safety and therapeutic potential of right ear or bilateral stimulation (Yap et al., 2020; Kim et al., 2022; Peng et al., 2023). In our original experimental design, we investigated potential differences based on the stimulation side (left vs. right ear groups); however, no significant differences in behavioral performance were found (Supplementary Table 1). Consequently, we merged the two groups to enhance statistical power for subsequent analyses. Given the preference for left ear stimulation, a clear evaluation of the stimulation side remains unachieved, indicating the need for further research to carefully assess the effects of taVNS on cognitive enhancement from this perspective.

Regarding the active/sham conditions, we targeted the cymba conchae for the active condition and applied stimulation to the same area for a short duration for the sham condition. However, there is still considerable debate regarding the target area and application methods. For active stimulation, in addition to the cymba conchae, other areas such as the cavum conchae, tragus, and antihelix have been targeted for various applications, including epilepsy, depression, and tinnitus, and have shown effects due to ABVN stimulation (Yap et al., 2020; Kim et al., 2022). For sham stimulation, active control methods primarily have involved stimulating the ear lobe or superior scapha, which have been considered to minimize innervation of the ABVN (Yap et al., 2020; Kim et al., 2022). However, recent studies have reported that such sham stimulation can yield effects comparable to active stimulation targeting the ABVN, not only in terms of brain activation patterns but also in neurophysiological indicators, including pupillary responses and cardiac vagal activity (Burger et al., 2020; Borges et al., 2021). As alternatives to active control for the sham condition, differentiated approaches such as passive control—where electrodes are attached but no stimulation is delivered—stimulation with very low frequencies (e.g., 1 Hz), and short-term stimulation have been explored (Ludwig et al., 2021; Chen et al., 2023; Badran et al., 2019; Rangon, 2018). Nevertheless, the validity of these approaches is still under discussion (Ludwig et al., 2021; Butt et al., 2020). In this study, we adopted a strategy to apply stimulation only during the first and last 30 s of the experimental session in order to explicitly avoid stimulation of the ABVN while incorporating placebo manipulation (Sun et al., 2021). However, it still has a limitation in that, considering the continuous sensations experienced by participants due to the stimulation, it might be distinguishable from the active condition. Thus, systematic analytical studies based on extensive experimental data are required to specify the target area and sham condition in taVNS. Furthermore, considering the variations in efficacy associated with stimulation parameters (Thakkar et al., 2025), it is necessary to establish a standardized taVNS protocol through comprehensive validation of stimulation parameters.

The virtual brain simulation has elicited meaningful outcomes by linking experimental findings with age-related white matter decline, suggesting that the modulation effects of taVNS may vary depending on the strength of structural connectivity in the brain. It has also demonstrated changes in functional characteristics (especially, FC changes) induced by taVNS at the whole-brain level, extending beyond the PFC, which can be analyzed based on fNIRS recordings (Supplementary Figure 4). However, validation studies based on extensive empirical data are still essential. Combining neuroimaging methods, such as fMRI or EEG/Magnetoencephalography (MEG), to observe neural responses induced by taVNS at the whole-brain level is crucial for optimizing the virtual brain model. Meanwhile, this study utilized standard structural MRI and normative connectome data due to the absence of individual MRI data, which prevented the reflection of each individual's structural brain characteristics. Personalized virtual brain models that accurately mimic the characteristics of brain networks based on individual structural and functional brain images can facilitate a more precise investigation of the modulation effects of taVNS in individual environments.

The current study focused on identifying the acute effects of taVNS. The observed acute effects on task performance and prefrontal FC (in the low-performance group) are quite promising. However, considering that most neuromodulation therapies primarily achieve plasticity changes and long-term effects through repetitive stimulations, in-depth analyses of longitudinal changes in brain networks conducted alongside behavioral experiments following repetitive stimulation sessions are crucial for elucidating the mechanism of taVNS.

Digital brain research can contribute to understanding the modulatory mechanisms of taVNS as an intervention for cognitive decline associated with aging or neurocognitive disorders, as well as to developing personalized strategies to optimize its effects, by integrating with behavioral assessments and brain signal analyses.

CRediT authorship contribution statement

Sora An: Writing – review & editing, Writing – original draft, Validation, Software, Methodology, Investigation, Funding acquisition, Formal analysis, Conceptualization. **Se Jin Oh:** Writing – review & editing, Resources, Data curation. **Shinhee Noh:** Resources, Data curation. **Sang Beom Jun:** Writing – review & editing, Validation, Supervision, Resources, Methodology, Funding acquisition, Conceptualization. **Jee Eun Sung:** Writing – review & editing, Validation, Supervision, Resources, Methodology, Funding acquisition, Conceptualization.

Declaration of competing interest

The authors declare that the research was conducted in the absence of any commercial or financial relationships that could be construed as a potential conflict of interest.

Funding

This research was supported by the Basic Science Research Program through the National Research Foundation of Korea (NRF) funded by the Ministry of Education (RS-2022-NR075832, RS-2023–00248701) and the Ministry of Science and ICT (MSIT) (RS-2022-NR070151, RS-2024–00461617). This research was also supported by the Bio&Medical Technology Development Program of the NRF funded by the Korean government (MSIT) (RS-2024–00401794) and the grant of the Korea Health Technology R&D Project through the Korea Health Industry Development Institute (KHIDI), which is funded by the Ministry of Health & Welfare, Republic of Korea (HI23C0156).

Supplementary materials

Supplementary material associated with this article can be found, in the online version, at doi:10.1016/j.neuroimage.2025.121179.

Data availability

Data will be made available on request.

References

Jodoin, V.D., Richer, F., Miron, J-P, Fournier-Gosselin, M-P, Lespérance, P., 2018. Long-term sustained cognitive benefits of vagus nerve stimulation in refractory depression. J. ECT. 34 (4), 283–290.

Sun, L., Peräkylä, J., Holm, K., Haapasalo, J., Lehtimäki, K., Ogawa, K.H., et al., 2017. Vagus nerve stimulation improves working memory performance. J. Clin. Exp. Neuropsychol. 39 (10), 954–964.

Wang, W., Li, R., Li, C., Liang, Q., Gao, X., 2024. Advances in VNS efficiency and mechanisms of action on cognitive functions. Front. Physiol. 15, 1452490.

Kong, Y., Zhao, K., Zeng, D., Lu, F., Li, X., Wu, Y., et al., 2024. Effects of vagus nerve stimulation on cognitive function in patients with epilepsy: a systematic review and meta-analysis. Front. Neurol. 15, 1332882.

Sjogren, M.J., Hellstrom, P.T., Jonsson, M.A., Runnerstam, M., Silander, HC-s, Ben-Menachem, E., 2002. Cognition-enhancing effect of vagus nerve stimulation in patients with Alzheimer's disease: a pilot study. J. Clin. Psych. 63 (11), 972–980.

Broncel, A., Bocian, R., Kłos-Wojtczak, P., Kulbat-Warycha, K., Konopacki, J., 2020. Vagal nerve stimulation as a promising tool in the improvement of cognitive disorders. Brain Res. Bull. 155, 37–47.

Austelle, C.W., Cox, S.S., Wills, K.E., Badran, BW., 2024. Vagus nerve stimulation (VNS): recent advances and future directions. Clin. Auto. Res. 1–19.

Badran, B.W., Austelle, CW., 2022. The future is noninvasive: a brief review of the evolution and clinical utility of vagus nerve stimulation. Focus. (Madison) 20 (1), 3–7.

Sharon, O., Fahoum, F., Nir, Y., 2021. Transcutaneous vagus nerve stimulation in humans induces pupil dilation and attenuates alpha oscillations. Journal of Neurosci. 41 (2), 320–330.

Jacobs, H.I., Riphagen, J.M., Razat, C.M., Wiese, S., Sack, AT., 2015. Transcutaneous vagus nerve stimulation boosts associative memory in older individuals. Neurobiol. Aging 36 (5), 1860–1867.

Wang, L., Zhang, J., Guo, C., He, J., Zhang, S., Wang, Y., et al., 2022. The efficacy and safety of transcutaneous auricular vagus nerve stimulation in patients with mild cognitive impairment: a double blinded randomized clinical trial. Brain Stimul. 15 (6), 1405–1414.

Trifilio, E., Shortell, D., Olshan, S., O'Neal, A., Coyne, J., Lamb, D., et al., 2023. Impact of transcutaneous vagus nerve stimulation on healthy cognitive and brain aging. Front. Neurosci. 17, 1184051.

Naparstek, S., Yeh, A.K., 2023. Mills-Finnerty C. Transcutaneous Vagus nerve stimulation (tVNS) applications in cognitive aging: a review and commentary. Front. Aging Neurosci. 15, 1145207.

Murphy, A.J., O'Neal, A.G., Cohen, R.A., Lamb, D.G., Porges, E.C., Bottari, S.A., et al., 2023. The effects of transcutaneous vagus nerve stimulation on functional connectivity within semantic and hippocampal networks in mild cognitive impairment. Neurotherapeutics. 20 (2), 419–430.

Badran, B.W., Dowdle, L.T., Mithoefer, O.J., LaBate, N.T., Coatsworth, J., Brown, J.C., et al., 2018. Neurophysiologic effects of transcutaneous auricular vagus nerve stimulation (taVNS) via electrical stimulation of the tragus: a concurrent taVNS/fMRI study and review. Brain Stimul. 11 (3), 492–500.

Fischer, R., Ventura-Bort, C., Hamm, A., Weymar, M., 2018. Transcutaneous vagus nerve stimulation (tVNS) enhances conflict-triggered adjustment of cognitive control. Cogn, Affect. Behav. Neurosci. 18, 680–693.

Kamoga, R., Rukundo, G.Z., Kalungi, S., Adriko, W., Nakidde, G., Obua, C., et al., 2024. Vagus nerve stimulation in dementia: a scoping review of clinical and pre-clinical studies. AIMS. Neurosci. 11 (3), 398.

Zhu, S., Liu, Q., Zhang, X., Zhou, M., Zhou, X., Ding, F., et al., 2024. Transcutaneous auricular vagus nerve stimulation enhanced emotional inhibitory control via increasing intrinsic prefrontal couplings. Int. J. Clin. Heal. Psychol. 24 (2), 100462.

Oh SJ, Noh S, Shin J, Jun SB, Sung JE. taVNS selectively enhances working memory in older adults with lower baseline performance, submitted.

Sun, J-B, Cheng, C., Tian, Q-Q, Yuan, H., Yang, X-J, Deng, H., et al., 2021. Transcutaneous auricular vagus nerve stimulation improves spatial working memory in healthy young adults. Front. Neurosci. 15, 790793.

Wright, H.H., Downey, R.A., Gravier, M., Love, T., Shapiro, L.P., 2007. Processing distinct linguistic information types in working memory in aphasia. Aphasiology. 21 (6–8), 802–813.

Christensen, S.C., Wright, HH., 2010. Verbal and non-verbal working memory in aphasia: what three n-back tasks reveal. Aphasiology. 24 (6–8), 752–762.

Shepard, R.N., Metzler, J., 1971. Mental rotation of three-dimensional objects. Science (1979) 171 (3972), 701–703.

Walter S, Amy E, Anthony Z. E-Prime User's Guide. Pittsburgh: Psychology Software Tools. 2002.

Schneider W, Eschman A, Zuccolotto A. E-Prime Reference Guide: Psychology Software Tools, Incorporated; 2002.

Huppert, T.J., Diamond, S.G., Franceschini, M.A., Boas, DA., 2009. HomER: a review of time-series analysis methods for near-infrared spectroscopy of the brain. Appl. Opt. 48 (10), D280–DD98.

Lin, S., Zhao, H., Duan, H., 2023. Brain-to-brain synchrony during dyadic action co-representation under acute stress: evidence from fNIRS-based hyperscanning. Front. Psychol. 14, 1251533.

Villringer, A., Chance, B., 1997. Non-invasive optical spectroscopy and imaging of human brain function. Trends. Neurosci. 20 (10), 435–442.

Naito, T., Oka, K., Ishii, K., 2024. Hemodynamics of short-duration light-intensity physical exercise in the prefrontal cortex of children: a functional near-infrared spectroscopy study. Sci. Rep. 14 (1), 15587.

Pedersen, M., Omidvarnia, A., Zalesky, A., Jackson, GD., 2018. On the relationship between instantaneous phase synchrony and correlation-based sliding windows for time-resolved fMRI connectivity analysis. Neuroimage 181, 85–94.

An, S., Fousek, J., Kiss, Z.H., Cortese, F., van Der Wijk, G., McAusland, L.B., et al., 2022. High-resolution virtual brain modeling personalizes deep brain stimulation for treatment-resistant depression: spatiotemporal response characteristics following stimulation of neural fiber pathways. Neuroimage 249, 118848.

Fonov, V.S., Evans, A.C., McKinstry, R.C., Almli, C.R., Collins, D., 2009. Unbiased nonlinear average age-appropriate brain templates from birth to adulthood. Neuroimage 47, S102.

Fonov, V., Evans, A.C., Botteron, K., Almli, C.R., McKinstry, R.C., Collins, D.L., et al., 2011. Unbiased average age-appropriate atlases for pediatric studies. Neuroimage 54 (1), 313–327.

Elias, G.J., Germann, J., Joel, S.E., Li, N., Horn, A., Boutet, A., et al., 2024. A large normative connectome for exploring the tractographic correlates of focal brain interventions. Sci. Data 11 (1), 353.

FreeSurfer, Fischl B., 2012. Neuroimage 62 (2), 774–781.

Montbrió, E., Pazó, D., Roxin, A., 2015. Macroscopic description for networks of spiking neurons. Phy. Rev. X 5 (2), 021028.

Lavanga, M., Stumme, J., Yalcinkaya, B.H., Fousek, J., Jockwitz, C., Sheheitli, H., et al., 2023. The virtual aging brain: causal inference supports interhemispheric dedifferentiation in healthy aging. Neuroimage 283, 120403.

Fousek, J., Rabuffo, G., Gudibanda, K., Sheheitli, H., Jirsa, V., eS, Petkoski, 2022. The structured flow on the brain's resting state manifold. bioRxiv. 1–20.

Hashemi, M., Ziaeemehr, A., Woodman, M.M., Fousek, J., Petkoski, S., Jirsa, VK., 2024. Simulation-based inference on virtual brain models of disorders. Mach. Learn. Sci. Technol. 5 (3), 035019.

Rabuffo, G., Fousek, J., Bernard, C., Jirsa, V., 2021. Neuronal cascades shape whole-brain functional dynamics at rest. eNeuro 8 (5).

Trebaul, L., Deman, P., Tuyisenge, V., Jedynak, M., Hugues, E., Rudrauf, D., et al., 2018. Probabilistic functional tractography of the human cortex revisited. Neuroimage 181, 414–429.

Spiegler, A., Hansen, E.C., Bernard, C., McIntosh, A.R., Jirsa, VK., 2016. Selective activation of resting-state networks following focal stimulation in a connectome-based network model of the human brain. eNeuro 3 (5).

Hilz, MJ., 2022. Transcutaneous vagus nerve stimulation-a brief introduction and overview. Auton. Neurosci. 243, 103038.

Colzato, L., Beste, C., 2020. A literature review on the neurophysiological underpinnings and cognitive effects of transcutaneous vagus nerve stimulation: challenges and future directions. J. Neurophysiol.

Levinson, S., Miller, M., Iftekhar, A., Justo, M., Arriola, D., Wei, W., et al., 2023. A structural connectivity atlas of limbic brainstem nuclei. Front. NeuroimAging 1, 1009399.

Friston, K.J., Harrison, L., Penny, W., 2003. Dynamic causal modelling. Neuroimage 19 (4), 1273–1302.

Aasted, C.M., Yücel, M.A., Cooper, R.J., Dubb, J., Tsuzuki, D., Becerra, L., et al., 2015. Anatomical guidance for functional near-infrared spectroscopy: atlasViewer tutorial. Neurophotonics. 2 (2), 020801. -.

Pfeifer, M.D., Scholkmann, F., Labruyère, R., 2018. Signal processing in functional near-infrared spectroscopy (fNIRS): methodological differences lead to different statistical results. Front. Hum. Neurosci. 11, 641.

Hampson, M., Driesen, N.R., Skudlarski, P., Gore, J.C., Constable, RT., 2006. Brain connectivity related to working memory performance. Journal of Neurosci. 26 (51), 13338–13343.

Jobson, D.D., Hase, Y., Clarkson, A.N., Kalaria, RN., 2021. The role of the medial prefrontal cortex in cognition, ageing and dementia. Brain Commun. 3 (3), fcab125.

de Oliveira Jereissati, L., da Silva, L.A., Antoniol, T., VO, Coimbra, da Silva, A.A., de Menezes, A.R.B., et al., 2023. The role of medial prefrontal cortex in cognition, aging and Parkinson disease. Braz. J. Clin. Med. Rev. 1 (3), 28–40.

Andrews-Hanna, J.R., Snyder, A.Z., Vincent, J.L., Lustig, C., Head, D., Raichle, M.E., et al., 2007. Disruption of large-scale brain systems in advanced aging. Neuron 56 (5), 924–935.

Xu, P., Chen, A., Li, Y., Xing, X., Lu, H., 2019. Medial prefrontal cortex in neurological diseases. Physiol. Genom. 51 (9), 432–442.

Dugré, J.R., Dumais, A., Tikasz, A., Mendrek, A., Potvin, S., 2021. Functional connectivity abnormalities of the long-axis hippocampal subregions in schizophrenia during episodic memory. npj Schizophrenia 7 (1), 19.

Boon, P., Vonck, K., van Rijckevorsel, K., El Tahry, R., Elger, C.E., Mullatti, N., et al., 2015. A prospective, multicenter study of cardiac-based seizure detection to activate vagus nerve stimulation. Seizure 32, 52–61.

Vespa, S., Heyse, J., Stumpp, L., Liberati, G., Santos, S.F., Rooijakkers, H., et al., 2021. Vagus nerve stimulation elicits sleep EEG desynchronization and network changes in responder patients in epilepsy. Neurotherapeutics. 18 (4), 2623–2638.

Thakkar, V.J., Crupper, J.E., Engelhart, A.S., Centanni, TM., 2025. Parameter optimization of non-invasive vagus nerve stimulation for second language learning in typically developing young adults. J. Neurolinguist. 73, 101225.
Ghasemian-Shirvan, E., Farnad, L., Mosayebi-Samani, M., Verstraelen, S., Meesen, R.L., Kuo, M-F, et al., 2020. Age-related differences of motor cortex plasticity in adults: a transcranial direct current stimulation study. Brain Stimul. 13 (6), 1588–1599.
Martí-Juan, G., Sastre-Garriga, J., Martinez-Heras, E., Vidal-Jordana, A., Llufriu, S., Groppa, S., et al., 2023. Using the Virtual Brain to study the relationship between structural and functional connectivity in patients with multiple sclerosis: a multicenter study. Cerebral Cortex 33 (12), 7322–7334.
Petkoski, S., Ritter, P., Jirsa, VK., 2023. White-matter degradation and dynamical compensation support age-related functional alterations in human brain. Cerebral Cortex 33 (10), 6241–6256.
Groh, J., Simons, M., 2024. White matter aging and its impact on brain function. Neuron.
Gunning-Dixon, F.M., Brickman, A.M., Cheng, J.C., Alexopoulos, GS., 2009. Aging of cerebral white matter: a review of MRI findings. Int. J. Geriat. Psych.: J. Psych. Late Life Allied Sci. 24 (2), 109–117.
Coelho, A., Fernandes, H.M., Magalhães, R., Moreira, P.S., Marques, P., Soares, J.M., et al., 2021. Signatures of white-matter microstructure degradation during aging and its association with cognitive status. Sci. Rep. 11 (1), 4517.
Yap, J.Y., Keatch, C., Lambert, E., Woods, W., Stoddart, P.R., Kameneva, T., 2020. Critical review of transcutaneous vagus nerve stimulation: challenges for translation to clinical practice. Front. Neurosci. 14, 284.
Kim, A.Y., Marduy, A., de Melo, P.S., Gianlorenco, A.C., Kim, C.K., Choi, H., et al., 2022. Safety of transcutaneous auricular vagus nerve stimulation (taVNS): a systematic review and meta-analysis. Sci. Rep. 12 (1), 22055.
Peng, X., Baker-Vogel, B., Sarhan, M., Short, E.B., Zhu, W., Liu, H., et al., 2023. Left or right ear? A neuroimaging study using combined taVNS/fMRI to understand the interaction between ear stimulation target and lesion location in chronic stroke. Brain Stimul. 16 (4), 1144–1153.
Borges, U., Pfannenstiel, M., Tsukahara, J., Laborde, S., Klatt, S., Raab, M., 2021. Transcutaneous vagus nerve stimulation via tragus or cymba conchae: are its psychophysiological effects dependent on the stimulation area? Int. J. Psychophysiol. 161, 64–75.
Ludwig, M., Wienke, C., Betts, M.J., Zaehle, T., Hämmerer, D., 2021. Current challenges in reliably targeting the noradrenergic locus coeruleus using transcutaneous auricular vagus nerve stimulation (taVNS). Auton. Neurosci. 236, 102900.
Chen, Y., Lu, X., Hu, L., 2023. Transcutaneous auricular vagus nerve stimulation facilitates cortical arousal and alertness. Int. J. Environ. Res. Pub. Health 20 (2), 1402.
Badran, B.W., Alfred, B.Y., Adair, D., Mappin, G., DeVries, W.H., Jenkins, D.D., et al., 2019. Laboratory administration of transcutaneous auricular vagus nerve stimulation (taVNS): technique, targeting, and considerations. J. Visual. Exp.: JoVE (143). https://doi.org/10.3791/58984.
Rangon, C-M., 2018. Reconsidering sham in transcutaneous vagus nerve stimulation studies. Clin. Neurophysiol.: Offic. J. Int. Fed. Clin. Neurophysiol. 129 (11), 2501–2502.
Burger, A.M., D'Agostini, M., Verkuil, B., Van Diest, I., 2020. Moving beyond belief: a narrative review of potential biomarkers for transcutaneous vagus nerve stimulation. Psychophysiology 57 (6), e13571.
Butt, M.F., Albusoda, A., Farmer, A.D., Aziz, Q., 2020. The anatomical basis for transcutaneous auricular vagus nerve stimulation. J. Anat. 236 (4), 588–611.